Variation of Entrainment in Annular Jets

John M. Kuhlman*
West Virginia University, Morgantown, West Virginia

Mean velocity distributions for axisymmetric circular and annular jets entering a stagnant ambient have been obtained, from which centerline velocity decay and jet width growth data have been extracted. In all instances, linear width growth and inverse centerline velocity decay laws are observed in the far field. The annular jet results in enhanced near-field mixing, as indicated by a consistent inward shift of the virtual origin. Also, far-field centerline velocity decay and jet width growth occur more quickly for the annular jet than for the circular jet. This is true even when the data are rescaled using characteristic length and velocity scales formed from the integrated initial jet mass flux and momentum flux. More importantly, far-field entrainment rates for some annular jet configurations are increased by more than 40% relative to the circular jet entrainment rate. It is believed that this is the result of enhancement of the near-field wake vortex train in the lee of the centerbody used to create the annular jet.

Nomenclature

$b_{0.5}$ = jet semiwidth
D = nominal jet exit diameter (2.54 cm)
D_{ef} = effective jet diameter, Eq. (1)
F = jet momentum flux
K_1 = jet semiwidth growth rate
K_2 = centerline velocity decay rate
ℓ = characteristic length scale for incompressible, nonbuoyant jet, Eq. (2)
$\dot{m}$ = initial jet mass flux
p = jet exit pressure
Q = initial jet volume flux
R = gas constant
r = radial coordinate
T_0 = stagnation temperature
U = mean axial velocity
x = axial coordinate
γ = specific heat ratio
ρ = density

Introduction

SEVERAL different methods have been demonstrated to alter the entrainment rates for simple planar or circular jet geometries.[1-11] For smooth exit conditions at relatively low Reynolds numbers, increasing jet Reynolds number consistently results in a small (order of 10%) decrease in entrainment, for both circular[1-3] and planar[3,4] geometries. Jet exit turbulence level at fixed Reynolds number increases entrainment more significantly (20%)[3,5] for a planar jet. Swirl can result in a doubling of entrainment for the round jet.[6] Even larger increases of entrainment (as much as a factor of four) have been achieved for the planar jet due to unsteady, periodic forcing by either a small airfoil[7,8] or a fluidic nozzle approach.[9] Acoustic, periodic forcing of a circular jet increased entrainment somewhat, but only in the near field.[10] Similarly, for an axisymmetric jet having a nonuniform initial mean velocity profile (annular jet), near-field entrainment was enhanced somewhat, with little variation in entrainment in the far field.[11] Far-field velocity decay and width growth rates were the same as for a circular jet, but virtual origins were shifted inward.[11]

In the present work, results are presented for entrainment rates for annular jets, where not only is near-field mixing enhanced (as indicated by an inward shift of the virtual origin), but in one instance the far-field entrainment rate is increased by 43% relative to the round jet. It is believed that this enhanced entrainment is primarily the result of enhancement of the wake vortex train[12-15] in the annular jet, rather than due to any variation in behavior of the jet vortex train.[10,16-21] Similar results have recently been briefly presented in preliminary form in Ref. 3. Also, Tsang[22,23] has reported results for annular jets in a cross flow, where a related concept was used to reduce entrainment; however, actual entrainment rates were not measured in that work.

Apparatus

The present work was performed with the same flat plate, nozzle, and transducers used in Refs. 24 and 25. For this study, the plate was mounted horizontally between two laboratory tables 0.80 m (2.63 ft) from the floor. A 1.45 m (4.75 ft) diameter by 0.91 m (3 ft) high circular screen of mesh size 1.6 mm (0.063 in.) was placed symmetrically around the plate to damp out disturbances in the entrained jet flow due to room pressure variations caused by the opening or closing of building doors. Also, all data were taken at night when few people were using the building. The laboratory ceiling was 4.3 m (14 ft) above the plane of the flat plate. The plate was fitted with 226 static pressure taps located on rays emanating from the jet orifice center, for measurement of the jet-induced pressure distributions described in Refs. 24 and 25. The plate surface was smoothed and filled with epoxy, resulting in the removal of an elliptical low region in the plate around the jet, which had been created by continual polishing of the plate during previous studies (Refs. 26–28). This was necessary to insure a symmetrical pressure distribution on the plate surface.[24,25]

The jet exited perpendicular to the plate through a machined circular orifice 2.54 cm (1.00 in.) in diameter D. The nozzle center was located 0.6 m (2 ft) from the rounded edge of the plate halfway across the 0.915 m (3 ft) dimension of the plate. The air jet issued from a 0.14 m (0.466 ft) diameter plenum chamber supplied by an air compressor through a smoothly contoured 30:1 area ratio contraction nozzle. A sectional view of the plenum and nozzle is shown in Fig. 1. Jet mass flow rate was measured with a turbine-type flowmeter

Received March 10, 1986; presented as Paper 86-1111 at the AIAA/ASME Fourth Fluid Mechanics, Plasma Dynamics and Lasers Conference, Atlanta, GA, May 12–14, 1986. Copyright © American Institute of Aeronautics and Astronautics, Inc., 1986. All rights reserved.

* Visiting Associate Professor, Department of Mechanical and Aerospace Engineering. Member AIAA.

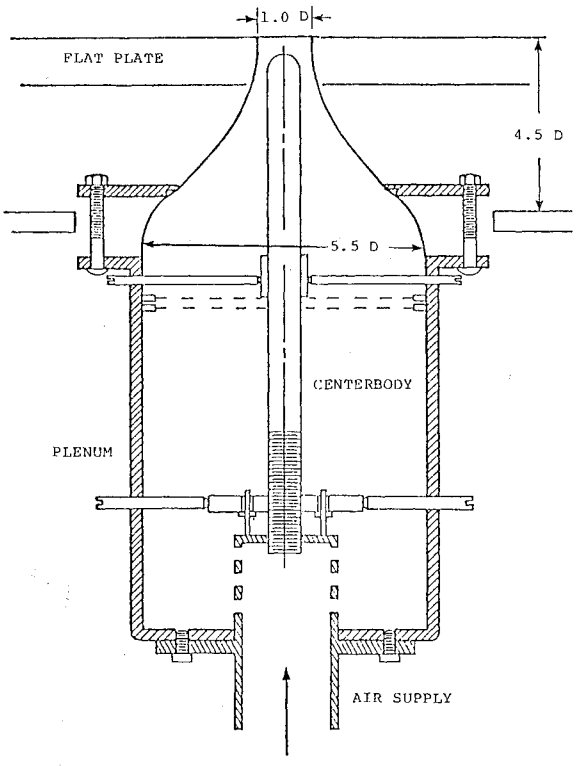

Fig. 1 Cross section of jet nozzle, plenum, and centerbody.

and held constant to within ±0.2% during any one run using an electronic feedback control, with jet plenum pressure and temperature and flowmeter rpm as inputs.

Also shown in Fig. 1 is one of the two centerbodies, or plugs, used to vary the jet exit plane dynamic pressure profiles and, hence, jet decay rate and width growth. The centerbody shown is cylindrical with a diameter of 1.9 cm (0.75 in. or 0.75 D), fitted with a hemispherical tip pointed in the jet flow direction. This centerbody is referred to herein as the hemispherical centerbody. A second centerbody or plug of the same diameter having a flat tip has also been used. Jet behavior has been altered by varying the submergence depth of the tips of these plugs beneath the jet exit/flat-plate plane, thereby resulting in an annular jet with a relatively low-momentum region on the jet axis.

A two-degrees-of-freedom traverse fitted with a 1.6 mm (0.0625 in.) diameter pitot static probe was clamped to a corner of the flat plate to measure jet dynamic pressures. Total and static pressure distributions were measured using a capacitance-type pressure transducer, digital electronic manometer, and chart recorder. The pressure transducer was calibrated using a dead weight tester. Temperatures of the jet and ambient air were monitored by 0.25 mm diameter chromel alumel thermocouples. Room air temperature was nominally 294 K (530°R), with jet exit temperatures nominally within 1 K (2°R) of the ambient temperature.

Experimental Procedure

The jet nozzle and plenum were physically aligned to be at right angles to the plate and were then rigidly mounted to the plate. This insured axial symmetry of the jet-induced plate static pressure distribution for the jet configuration with no centerbody. For nozzle configurations with a centerbody, the centerbody was first aligned mechanically with respect to the flat plate and nozzle and then, if necessary, adjusted slightly to yield both a symmetrical jet exit plane dynamic pressure distribution and a symmetrical plate surface pressure distribution. Jet exit plane dynamic pressure profiles were measured using the pitot static probe located 0.25 D above the jet exit plane. Airflow rates for each nozzle/centerbody configuration were adjusted so that maximum jet exit dynamic pressures were held nearly constant for all configurations. The maximum jet exit Mach number was nominally 0.4 and the Reynolds number based on maximum dynamic pressure and D was nominally 2.7×10^5.

For the various nozzle/centerbody configurations calibrated as described above, the jet centerline dynamic pressure decay and lateral mean velocity profiles were measured using the pitot static probe and traverse. Also, for each of these nozzle/centerbody configurations, the jet-induced static pressures on the plate surface were measured using the pressure transducer, manometer, and recorder, as described in Refs. 24 and 25. In the present work, the lateral profiles of mean velocity have been graphically analyzed to extract jet width information for each configuration. Jet semiwidth $b_{0.5}$, has been defined herein as the local jet radius at which the measured axial velocity equals one-half of the centerline value. From the measured centerline velocity and jet semiwidth data, far-field entrainment rates have also been calculated.

Results

All basic results of the present work are presented in the form of centerline velocity decay curves in Figs. 2 and 3, along with jet width growth curves in Fig. 4. In Fig. 2 the inverse of the maximum jet velocity, normalized by the maximum jet exit velocity, is shown vs the axial distance normalized by the nominal jet exit diameter, $D = 2.54$ cm. These data have been taken from Refs. 24 and 25 and replotted in the present form to emphasize the proportionality between $U(x)$ and $(x)^{-1}$ in the fully developed region of the jet. In Fig. 2a, annular jet configurations due to a flat-tipped centerbody are compared with the round jet. It is seen that all flat-tip annular jets have more rapid centerline velocity decay than the round jet and that all annular jet centerline velocity decay curves are quite close to one another when plotted vs x/D. Least squares curve fits to the linear portions of these curves yield $U(0)/U(x) = 0.144(x/D + 0.87)$ for the round jet and an average centerline velocity equation of $U(0)/U(x) = 0.250(x/D + 1.56)$ for the four annular jets. It is thus seen that the annular jets have quicker centerline velocity decay, as well as a slight inward shift of the virtual origin for centerline velocity decay.

Figure 2b presents similar data for the hemispherical-tipped centerbody, again compared with the round jet. Again, all of these annular jet configurations have more rapid centerline velocity decay than the round jet and an inward shift of the virtual origin. However, it is noted that, while two configurations (flush and 1.0 D down) have essentially the same centerline velocity decay as the flat-tipped centerbody results (Fig. 2a), one of these annular jets (the 0.5 D down configuration) has an even faster centerline velocity decay. Here, curve fits to the first two hemispherical-tipped configurations yield an average decay equation of $U(0)/U(x) = 0.260(x/D + 1.62)$, very close to the average behavior for all flat-tipped configurations. The hemispherical centerbody down 0.5 D, on the other hand, yields a far-field decay of $U(0)/U(x) = 0.323(x/D + 1.25)$.

While these results highlight the more rapid decay of the annular jet centerline velocity in physical coordinates, they do not present a logical comparison, since the round jet diameter D is not a proper choice of characteristic length scale for the annular jet configurations. Instead, an effective diameter D_{ef} of an equivalent round jet, having the same mass flux and momentum flux as the annular jet, must be used. As developed by Ziegler and Wooler,[29] this equivalent round jet diameter is calculated based on isentropic expansion to a uniform velocity from the same stagnation state to the same exit pressure as the annular jet, with the same mass and momentum fluxes, so that[29]

$$D_{ef} = \sqrt{\frac{2F\left[2RT_0 - (\gamma - 1)(F/\dot{m})^2/\gamma\right]}{\pi p (F/\dot{m})^2}} \qquad (1)$$

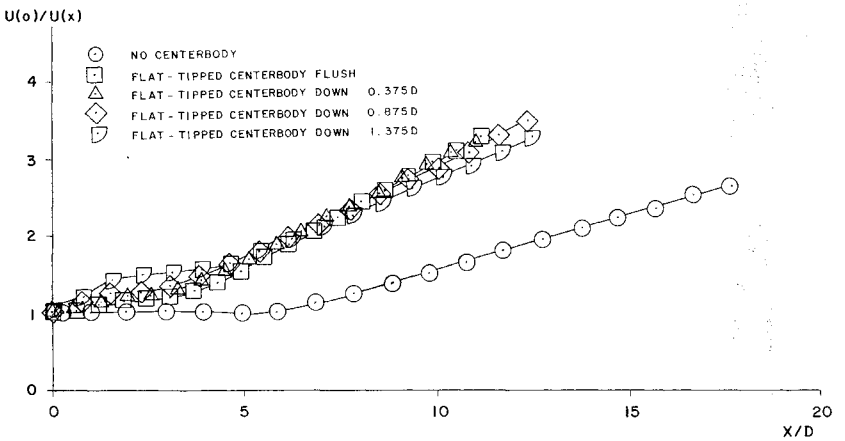

Fig. 2a Inverse of centerline velocity decay vs axial distance normalized by nomial jet diameter D: flat-tipped centerbody jets compared with circular jet.

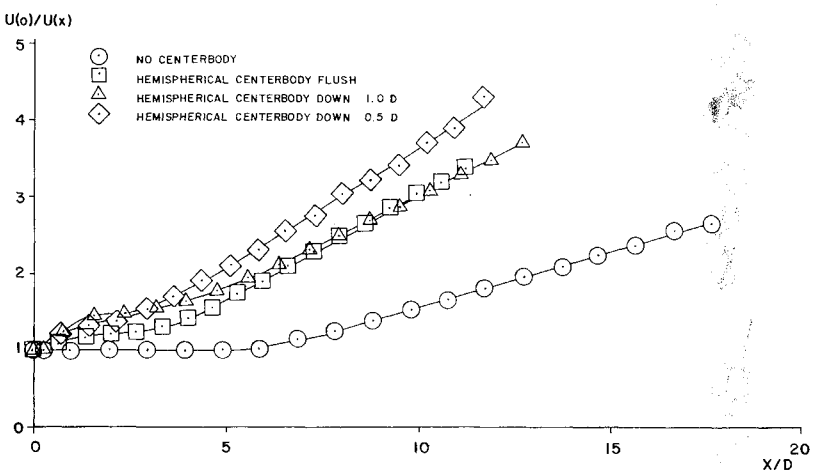

Fig. 2b Inverse of centerline velocity decay vs axial distance normalized by nominal jet diameter D: hemispherical-tipped centerbody jets compared with circular jet.

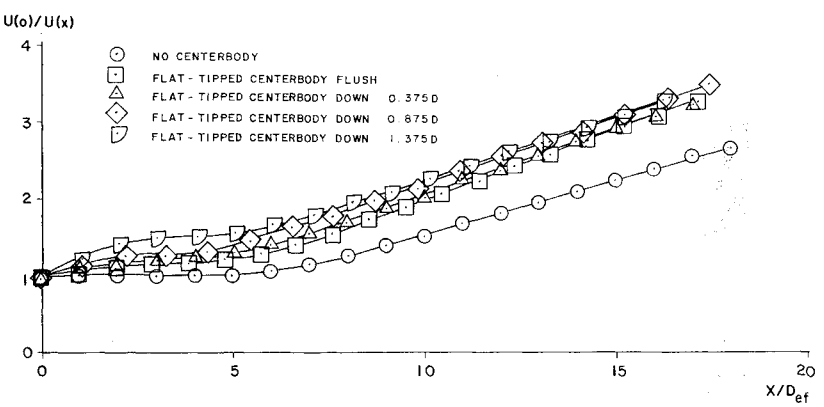

Fig. 3a Inverse of centerline velocity decay vs axial distance normalized by effective jet diameter D_{ef}: comparison between circular and annular jets due to flat-tipped centerbody.

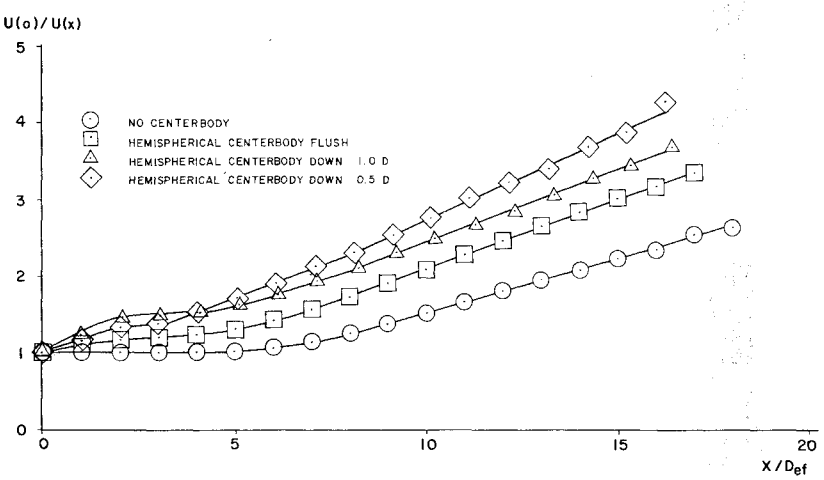

Fig. 3b Inverse of centerline velocity decay vs axial distance normalized by effective jet diameter D_{ef}: comparison between circular and annular jets due to hemispherical-tipped centerbody.

where F is the jet momentum flux or thrust, p the exit pressure, and T_0 the stagnation temperature. Here, F has been calculated from graphical integration of the jet exit velocity times the local radius. A similar procedure was used earlier by Chigier and Beér[11] in their annular jet work. This length scale has been used in earlier work by the author.[24-28] It should be noted that this choice of characteristic length scale for the annular jet is essentially equivalent to that used in the hydraulics literature,[30,31] where a characteristic jet length scale is formed via dimensional analysis from the initial volume flux Q and kinematic momentum flux F/ρ as

$$\ell = Q/(F/\rho)^{1/2} \tag{2}$$

The centerline velocity data from Fig. 2 have been replotted vs x/D_{ef} in Fig. 3. Visual inspection of these data for the flat-tipped centerbody configurations (Fig. 3a) indicates that when correct comparisons between the annular jets and the round jet are made using D_{ef}, the major difference is an inward shift of the virtual origin for the annular jet, while far-field decay rate is not greatly different. More careful comparisons are possible using the least squares curve fit equations to the linear portions of the curves in Fig. 3a, as given in Table 1. Here it is seen that, on average, for the annular jet configurations the virtual origin is shifted inward approximately 1.4 D_{ef}, while the far-field centerline velocity decay rate is slightly higher (22%) than for the round jet. This same trend of inward shift of the virtual origins for annular jets was also seen by Chigier and Beér.[11]

Similar centerline velocity results are shown in Fig. 3b for the hemispherical-tipped centerbody annular jets. Here, even with the proper choice of characteristic length scale, there are clear trends toward both the inward shift of the virtual origin noted in Fig. 3a and a significant increase in far-field centerline velocity decay rate, as shown in Table 1. The flush and 1.0 D down hemispherical centerbody configurations have virtual origins and decay rates similar to the flat-tipped centerbody configurations. However, the far-field centerline velocity decay rate for the 0.5 D down hemispherical centerbody configuration is 65% higher than for the round jet.

The above data have been presented previously in Refs. 24 and 25, although they have not been analyzed as herein. The new data presented in the present work is summarized in Fig. 4, where the measured variations of jet semiwidth $b_{0.5}$, have been presented for all annular jet configurations for which centerline velocity decay measurements are shown in Figs. 2 and 3. The jet semiwidth has been defined here as the radial location where the local mean axial velocity equals one-half of the maximum value at each axial position. These new results have been graphically extracted from lateral traverses of mean axial velocity at several axial stations for each jet configuration. In Fig. 4, both the jet semiwidth and axial coordinate have been normalized by the appropriate characteristic length scale D_{ef}. All jet width growth rates calculated from these

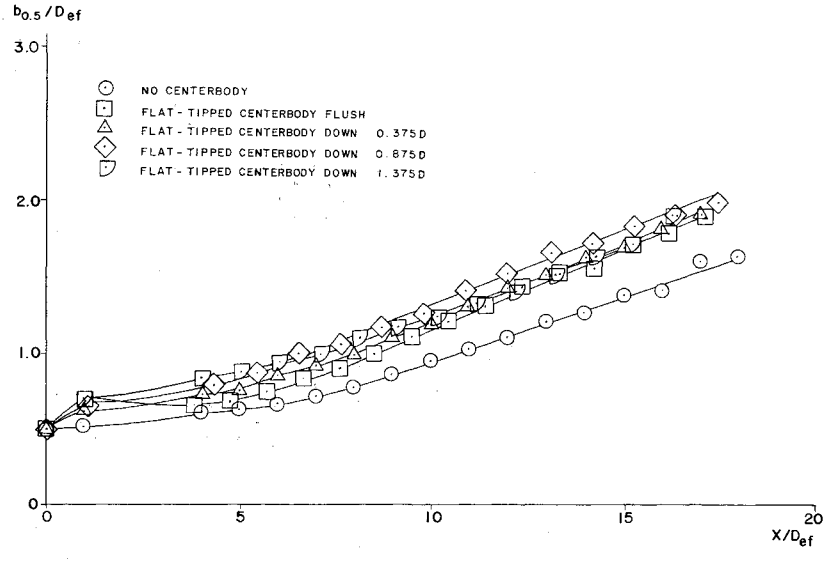

Fig. 4a Jet semiwidth vs axial distance, both normalized by effective jet diameter D_{ef}: comparison between circular and annular jets due to flat-tipped centerbody.

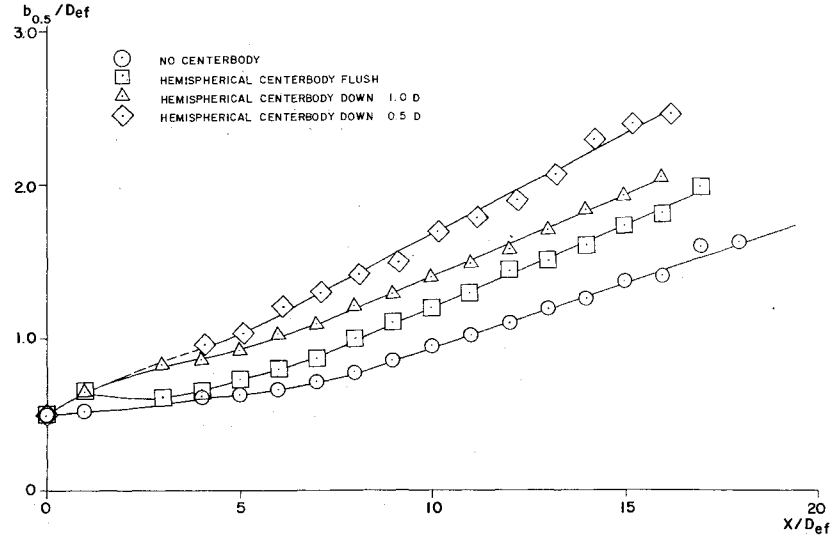

Fig. 4b Jet semiwidth vs axial distance, both normalized by effective jet diameter D_{ef}: comparison between circular and annular jets due to hemispherical tipped centerbody.

Table 1 Far-field centerline velocity decay and jet width growth variation for round and annular jet configurations

Configuration	Centerline velocity decay, $U(0)/U(x)$	Width growth, $b_{0.5}/D_{ef}$
Round jet	$0.141(x/D_{ef}+0.884)$	$0.0859(xD_{ef}+1.02)$
Flat-tip flush	$0.183(x/D_{ef}+0.821)$	$0.1039(x/D_{ef}+1.15)$
Flat-tip 0.375 D down	$0.169(x/D_{ef}+2.127)$	$0.099(x/D_{ef}+2.18)$
Flat-tip 0.875 D down	$0.173(x/D_{ef}+2.635)$	$0.0962(x/D_{ef}+3.58)$
Flat-tip 1.375 D down	$0.164(x/D_{ef}+3.617)$	$0.0963(x/D_{ef}+2.82)$
Flat-tip average	$0.172(x/D_{ef}+2.30)$	$0.0988(x/D_{ef}+2.33)$
Hemi-tip flush	$0.182(x/D_{ef}+1.58)$	$0.1079(x/D_{ef}+1.16)$
Hemi-tip 1.0 D down	$0.190(x/D_{ef}+2.85)$	$0.1040(x/D_{ef}+3.26)$
Hemi-tip 0.5 D down	$0.233(x/D_{ef}+1.73)$	$0.1321(x/D_{ef}+2.65)$

Table 2 Far-field entrainment rates for annular jets compared to round jet

Configuration	Entrainment rate, $4(1.20)^2K_1^2/K_2$	Change, %
Round jet (present)	0.303	—
Flat-tip flush	0.340	+12
Flat-tip 0.375 D down	0.335	+11
Flat-tip 0.875 D down	0.308	+2
Flat-tip 1.375 D down	0.326	+8
Hemi-tip flush	0.369	+22
Hemi-tip 1.0 D down	0.328	+8
Hemi-tip 0.5 D down	0.432	+43

results are identical to those which would be obtained from curve fits to plots of jet width vs x in physical coordinates.

Jet semiwidth results for the flat-tipped centerbody configurations are compared with jet semiwidth for the round jet in Fig. 4a. Jet width growth is linear beyond about $x/D_{ef}=5$. It appears that all flat-tipped centerbody annular jets have approximately the same width growth rate as the round jet, with an inward shift of virtual origin being the major difference from the round jet. This is confirmed by comparison of the far-field jet width growth equations given in Table 1, again obtained from least squares curve fits to the far-field, linear width growth data. The jet width virtual origin shifts inward approximately 1.5 D_{ef}, on average, for the flat-tipped centerbody configurations, while the average width growth rate is 15% higher than the round jet value.

The corresponding jet semiwidth results for the hemispherical-tip centerbody are compared with the round jet width in Fig. 4b. Again, width growth is linear beyond $x/D_{ef}=5$ and the annular jet configurations consistently display an inward shift of the jet width virtual origin. However, there is also a clear difference between far-field width growth rates for the hemispherical-tip centerbody annular jets and the round jet. Here, these annular jets have significantly higher growth rates, as detailed in Table 1. Note that the 0.5 D down configuration has a 54% more rapid far-field width growth rate than the round jet. This data set for the hemispherical-tip centerbody annular jets is the key result in the present work, where it is seen that far-field velocity decay rate is increased by 65% and width growth rate is increased by 54%, for this one configuration.

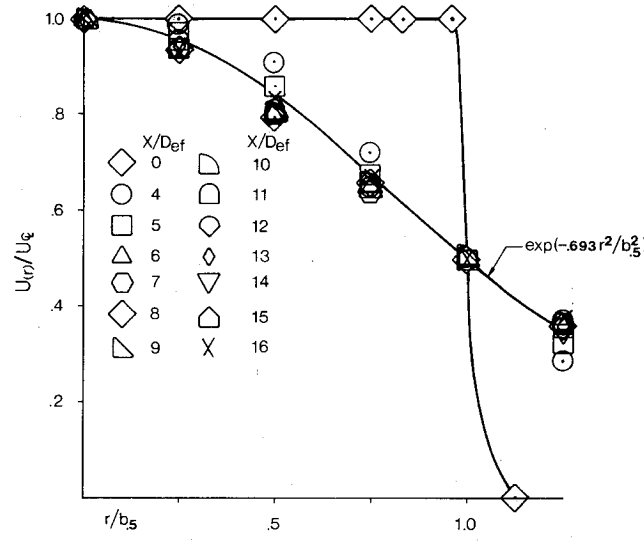

Fig. 5a Lateral profiles of mean velocity for round jet (no centerbody).

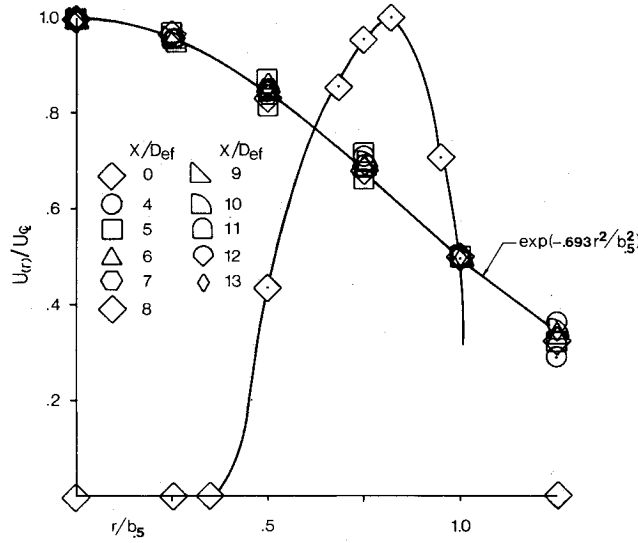

Fig. 5b Lateral profiles of mean velocity for hemispherical centerbody down 0.5D configuration.

Discussion and Conclusions

As described previously in Ref. 3, it is possible to calculate far-field entrainment rates by assuming the far-field mean velocity profiles to be similar. Then, ignoring the virtual origins in the centerline velocity decay and width growth relationships (Table 1) and assuming Gaussian lateral profiles, the jet volume flux should be proportional to

$$Q(x) \sim \pi\left(K_1^2/K_2\right)(x/D_{ef}) \qquad (3)$$

where K_1 is the jet width growth rate and K_2 the centerline velocity decay rate. Thus, the quantity $\pi K_1^2/K_2$ becomes a measure of the entrainment rate into the jet in the far field. Note that the present technique[3] for calculating far-field entrainment rates differs from previous methods either by direct measurement of the entrained flow[1,32] or by integration of measured lateral profiles of mean velocity, either faired to zero or terminated at a radial location where the mean velocity is a constant fraction of the local centerline value.[33]

Typical examples of measured lateral profiles of mean velocity are shown in Fig. 5a for the round jet and Fig. 5b for the hemispherical centerbody down $0.5D$ configuration to illustrate the observed similarity beyond approximately $x/D_{ef} = 5$. Note that estimated measurement errors result in uncertainties in $U(r)/U(0)$ ranging from 5% near the centerline to 15% beyond $r = b_{0.5}$.

The calculated far-field entrainment rates have been tabulated in Table 2 for all annular jet configurations studied and are compared with the corresponding round jet value from the present work. However, note that the present experimental results have presented jet semiwidth $b_{0.5}$ results where the local velocity equals one-half of the centerline value. Instead, if Gaussian lateral profiles are assumed, the appropriate jet semiwidth is the location where the velocity equals $1/e$ times the centerline value. This width is a constant factor of 1.2011 times larger than $b_{0.5}$. Also, to properly normalize $Q(x)$ such that $Q(0) = 1$, the volume flux expression, Eq. (3) should be multiplied by a factor of $(4/\pi)$. The actual far-field entrainment rate is then equal to $4(1.2011)^2K_1^2/K_2$. The present calculated far-field entrainment rate for the round jet of 0.303 compares favorably with the direct entrainment measurements of Ricou and Spalding[1] and Hill.[32] In both of these studies, a far-field entrainment rate coefficient of 0.32 was measured. It is noted that the far-field entrainment rates for all annular jet configurations are consistently higher than the entrainment rate for the round jet. This consistent increase in far-field entrainment rate is in addition to the apparently increased near-field entrainment, as indicated by the shortening of a zone of flow establishment and the inward shift of the virtual origins for centerline velocity decay and jet width growth. It is this increased far-field entrainment rate for the annular jet, by as much as 43% compared to an equivalent, uniform, round jet, that is the key result of the present work. These data demonstrate one passive means by which significant increases in jet mixing and entrainment may be achieved. A second approach is described in Ref. 34.

One plausible explanation for the physical mechanism for this entrainment increase might be found in recent studies of the coherent structures or vortex trains found in the near-field regions of round and annular jets.[10,12-21] First, the consistent and dramatic inward shift of the centerline velocity and jet width virtual origins, and (qualitatively) the attendant near-field entrainment increase, might be explained as resulting from enhancement of the effects due to the jet vortex train of toroidal vortices in the outer jet shear layer.[10,16-21] On the other hand, the increase in far-field entrainment by 43% over that of the round jet for the hemispherical-tipped centerbody down 0.5 D annular jet might be explained as resulting from enhancement of the wake vortex train[12-15] formed in the near field in the lee of the centerbody. This wake-induced vortex train was found by Ko and Lam[13] to dominate the jet vortices in the outer shear layer as the effects of the annular nature of the jet became more pronounced. These wake-induced vortices are apparently more pronounced for the hemispherical-tipped centerbody than for the flat-tipped centerbody. Previous measurements of the growth of wakes behind both axisymmetric[35] and two-dimensional[36] bodies support the present conclusion that the observed far-field entrainment increases are the result of enhancement of the wake-type vortices that form in the lee of the centerbody.

References

[1] Ricou, F.P. and Spalding, D.B., "Measurements of Entrainment by Axisymmetric Turbulent Jets," *Journal of Fluid Mechanics*, Vol. 11, 1961, pp. 21–32.

[2] Oosthuizen, P.H., "An Experimental Study of Low Reynolds Number Turbulent Circular Jet Flow," ASME Paper 83-FE-36, June 1983.

[3] Kuhlman, J.M., "Survey of Nearfield Reynolds Number Effects and Initial Condition Effects on Buoyant and Nonbuoyant Jets," *Proceedings, ASME-ASCE Int'l Symposium on Modeling Environmental Flows*, Book G00290, ASME, New York, June 1985, pp. 21–31.

[4] Lemieux, G.P. and Oosthuizen, P.H., "Experimental Study of the Behavior of Plane Turbulent Jets at Low Reynolds Numbers," AIAA Paper 84-1661, June 1984.

[5] Goldschmidt, V.W. and Bradshaw, P., "Effects of Nozzle Exit Turbulence on the Spreading (or Widening) Rate of Plane Free Jets," ASME Paper 81-FE-22, June 1981.

[6] Chigier, N.A. and Beér, J.M., "Velocity and Static-Pressure Distributions in Swirling Air Jets Issuing from Annular and Divergent Nozzles," *Transactions of ASME, Journal of Basic Engineering*, Vol. D86, Dec. 1964, pp. 788–796.

[7] Simmons, J.M., Lai, J.C.S., and Platzer, M.F., "Jet Excitation by an Oscillating Vane," *AIAA Journal*, Vol. 19, June 1981, pp. 673–676.

[8] Lai, J.C.S. and Simmons, J.M., "Instantaneous Velocity Measurements in a Vane-Excited Plane Jet," *AIAA Journal*, Vol. 23, Aug. 1985, pp. 1157–1164.

[9] Platzer, M.F., Simmons, J.M., and Bremhorst, K., "Entrainment Characteristics of Unsteady Subsonic Jets," *AIAA Journal*, Vol. 16, March 1978, pp. 282–284.

[10] Crow, S.C. and Champagne, F.H., "Orderly Structure in Jet Turbulence," *Journal of Fluid Mechanics*, Vol. 48, Pt. 3, 1971, pp. 547–591.

[11] Chigier, N.A. and Beér, J.M., "The Flow Region Near the Nozzle in Double Concentric Jets," *Transactions of ASME, Journal of Basic Engineering*, Vol. D86, Dec. 1964, pp. 797–804.

[12] Ko, N.W.M. and Chan, W.T., "The Inner Regions of Annular Jets," *Journal of Fluid Mechanics*, Vol. 93, Pt 3, 1979, pp. 549–584.

[13] Ko, N.W.M. and Lam, K.M., "Flow Structures of a Basic Annular Jet," *AIAA Journal*, Vol. 23, No. 8, Aug. 1985, pp. 1185–1190.

[14] Ko, N.W.M. and Davies, P.O.A.L., "The Near Field Within the Potential Cone of Subsonic Cold Jets," *Journal of Fluid Mechanics*, Vol. 50, Pt. 1, 1971, pp. 49–78.

[15] Ko, N.W.M. and Leung, K.C., "Covariance Measurements in the Initial Region of an Annular Jet," *Journal of Sound and Vibration*, Vol. 80, No. 3, 1982, pp. 339–354.

[16] Wille, R., "Beiträge zur Phänomenologie der Freistrahlen," *Zeitschrift für Fluswissenschaften*, Vol. 6, 1963, pp. 222–233.

[17] Bradshaw, P., Ferriss, D.H., and Johnson, R.F., "Turbulence in the Noise-Producing Region of a Circular Jet," *Journal of Fluid Mechanics*, Vol. 19, 1964, pp. 591–624.

[18] Becker, H.A. and Massaro, T.A., "Vortex Evolution in a Round Jet," *Journal of Fluid Mechanics*, Vol. 31, Pt. 3, 1968, pp. 435–448.

[19] Lau, J.C. and Fisher, M.J., "The Vortex-Street Structure of 'Turbulent' Jets, Part 1," *Journal of Fluid Mechanics*, Vol. 67, Pt. 2, 1975, pp. 299–337.

[20] Bruun, H.H., "A Time-Domain Analysis of the Large-Scale Flow Structure in a Circular Jet, Part 1, Moderate Reynolds Number," *Journal of Fluid Mechanics*, Vol. 83, Pt. 4, 1977, pp. 641–671.

[21] Sokolov, M., Kleis, S.J., and Hussain, A.K.M.F., "Coherent Structures Induced by Two Simultaneous Sparks in an Axisymmetric Jet," *AIAA Journal*, Vol. 19, Aug. 1981, pp. 1000–1008.

[22] Tsang, G., "Stack Exit Velocity Distribution for Higher Effective Stack Height," *Atmospheric Environment*, Vol. 6, Pergamon Press, New York, 1972, pp. 815–828.

[23] Tsang, G., "Further Laboratory Experiments on a Stack of Optimal Exit Velocity Distribution," *Atmospheric Environment*, Vol. 7, Pergamon Press, New York, 1973, pp. 755–762.

[24] Kuhlman, J.M. and Warcup, R.W., "Jet Decay Rate Effects on Hover Jet-Induced Loads," *Journal of Aircraft*, Vol. 17, Aug. 1980, pp. 605–607.

[25] Kuhlman, J.M. and Warcup, R.W., "Experimental Investigation of Jet-Induced Loads on a Flat Plate in Hover Out-of-Ground Effect," NASA CR-159004, Feb. 1979.

[26] Kuhlman, J.M. and Warcup, R.W., "Effects of Jet Decay Rate on Jet-Induced Loads on a Flat Plate," *Journal of Aircraft*, Vol. 15, May 1978, pp. 293–297.

[27] Kuhlman, J.M., Ousterhout, D.S., and Warcup, R.W., "Experimental Investigation of Effect of Jet Decay Rate on Jet-Induced Pressures on a Flat Plate," NASA CR-2979, April 1978.

[28] Kuhlman, J.M., Ousterhout, D.S., and Warcup, R.W., "Experimental Investigation of Effects of Jet Decay Rate on Jet-Induced Pressures on a Flat Plate: Tabulated Data," NASA CR-158990, Nov. 1978.

[29] Ziegler, H. and Wooler, P.T., "Analysis of Stratified and Closely Spaced Jets Exhausting into a Crossflow," NASA CR-132297, Nov. 1973.

[30] List, E.J. and Imberger, J., "Turbulent Entrainment in Buoyant Jets and Plumes," *Proceedings of ASCE, Journal of Hydraulics Division*, Vol. 99, No. HY9, Sept. 1973, pp. 1461–1474.

[31]Wright, S.J., "Mean Behavior of Buoyant Jets in a Crossflow," *Proceedings of ASCE, Journal of Hydraulics Division*, Vol. 103, No. HY5, May 1977, pp. 499–513.

[32]Hill, B.J., "Measurement of Local Entrainment Rate in the Initial Region of Axisymmetric Turbulent Air Jets," *Journal of Fluid Mechanics*, Vol. 51, Pt. 4, 1972, pp. 773–779.

[33]Trabold, T.A., Essen, E.B., and Obot, N.T., "Entrainment by Turbulent Jets Issuing from Sharp-Edged Inlet Round Nozzles," *Proceedings, ASME Int'l Symposium on Jets and Cavities*, Book FED-Vol. 31, ASME, New York, Nov. 1985, pp. 101–109.

[34]Wlezien, R.W. and Kibens, V., "Passive Control of Jets with Indeterminate Origins," *AIAA Journal*, Vol. 24, Aug. 1986, pp. 1263–1270.

[35]Bevilaqua, P.M. and Lykoudis, P.S., "Turbulence Memory in Self-Preserving Wakes," *Journal of Fluid Mechanics*, Vol. 89, Dec. 1978, pp. 589–606.

[36]Gray, D.D. and Sheldon, G.F., "Growth of Two-Dimensional Wakes Behind Solid and Porous Strips," *AIAA Journal*, Vol. 20, Jan. 1982, pp. 150–152.

From the AIAA Progress in Astronautics and Aeronautics Series...

SPACECRAFT CONTAMINATION: SOURCES AND PREVENTION – v. 91

Edited by J.A. Roux, The University of Mississippi
and
T.D. McCay, NASA Marshall Space Flight Center

This recent Progress Series volume treats a variety of topics dealing with spacecraft contamination and contains state-of-the-art analyses of contamination sources, contamination effects (optical and thermal), contamination measurement methods (simulated environments and orbital data), and contamination-prevention techniques. Chapters also cover causes of spacecraft contamination, and assess the particle contamination of the optical sensors during ground and launch operations of the Shuttle. The book provides both experimental and theoretical analyses (using the CONTAM computer program) of the contamination associated with the bipropellant attitude-control thrusters proposed for the Galileo spacecraft. The results are also given for particle-sampling probes in the near-field region of a solid-propellant rocket motor fired in a high-altitude ground test facility, as well as the results of the chemical composition and size distribution of potential particle contaminants.

Published in 1984, 333 pp., 6×9, illus., $39.50 Mem., $69.50 List; ISBN 0-915928-85-X

TO ORDER WRITE: Publications Dept., AIAA, 1633 Broadway, New York, N.Y. 10019